1-1-1989

An Algebraic Model for a Zinc/Bromine Flow Cell

G. D. Simpson
Texas A & M University - College Station

Ralph E. White
University of South Carolina - Columbia, white@cec.sc.edu

Publication Info

Journal of the Electrochemical Society, 1989, pages 2137-2144.

DOI: 10.1149/1.2097226
http://dx.doi.org/10.1149/1.2097226

An Algebraic Model for a Zinc/Bromine Flow Cell

G. D. Simpson* and R. E. White**

Department of Chemical Engineering, Texas A&M University, College Station, Texas 77843

ABSTRACT

An algebraic model for a parallel plate, zinc/bromine flow cell is presented and used to predict various performance quantities, which are compared to those predicted by using previously published differential equation models. The results presented compare well with previous work. The model is based on the concept of using well-mixed zones and linear concentration and potential profiles for the diffusion layers and the separator. The Butler-Volmer equation is used for the electrochemical reactions, and the homogeneous reaction between bromine and bromide is included.

A zinc/bromine battery consists essentially of two electrodes, a porous separator, and a pair of storage tanks. The separator is placed between the electrodes in such a way that there is a thin gap between each of the electrodes and the separator. An electrolytic solution containing Zn^{+2} and Br^- (among other things) is forced through the gaps between the electrodes and the separator. After the solution from each gap exits the reactor, it enters the associated storage tank and is recycled later to the reactor.

During charge, the principle reaction at the anode is the oxidation of Br^- to Br_2. At the cathode the principle reaction is the reduction of Zn^{+2} to Zn. An undesirable reaction at the cathode during charge is the reduction of Br_2 to Br^-. A homogeneous phase bulk reaction occurs between Br_2 and Br^- to yield Br_3^-. The two electrochemical reactions can be written in anodic form as

$$Br^- \rightleftharpoons \frac{1}{2} Br_2 + e^- \quad \text{Reaction 1}$$

$$Zn \rightleftharpoons \frac{1}{2} Zn^{+2} + e^- \quad \text{Reaction 2}$$

and the complexation reaction can be written as

$$Br^- + Br_2 \rightleftharpoons Br_3^- \quad \text{Reaction 3}$$

The equilibrium constant for this homogeneous reaction is 17,000 (cm^3/mol) (1).

Previous authors have modeled the zinc/bromine flow cell (2-7). Lee and Selman (2, 3) developed a model to determine the current density distribution along the electrode surfaces. Lee (4) extended that work to include time variations of the current density distribution in an attempt to predict dendrite formation. Van Zee *et al.* (5) developed a simplified model to describe overall cell performance. Mader and White (6) also developed a model that can be used to predict the overall cell performance by introducing a "one-step" approximation. Evans and White (7) extended that work by including a porous electrode and the capability of predicting round-trip energy efficiencies. Evans and White (8) present a review of the work done on the zinc/bromine flow cell.

Two basic approaches have dominated the modeling of parallel plate cells. The simpler of these approaches is to assume that the cell is operated under diffusion-limited conditions (9). This method can accurately predict the reactor's limiting current density and maximum conversions when the electrodes are operated at high overpotentials and the effects of ionic migration are negligible. The more general of these approaches is to write a series of governing equations that describe the reactor's performance under all conditions. The equations written are a set of partial differential equations that represent conservation of mass and a single algebraic equation that represents the electroneutrality condition. After the equations are written, they are solved numerically subject to applicable boundary conditions. The numerical solution requires that the partial differential equations be approximated by suitable finite-difference equations. These equations are then solved simultaneously to determine the various concentrations and potentials. The fundamentals of this technique are presented by Newman (10) and others (11, 12).

The model presented herein is an algebraic simplification of the second approach. In the model development it is assumed that the concentration profiles within the reactor can be approximated by a series of constant and linear regions and that the potential profiles can be approximated by a series of linear regions are shown in Fig. 1. The regions of constant concentration correspond with perfectly mixed regions in the bulk of the electrolyte. The regions where the concentration profiles are linear correspond with regions near the electrodes where both diffusion and migration are present. The potential profile is assumed to be linear through each region of the reactor. This algebraic approach to modeling a parallel plate flow cell results in a significant simplification over the more rigorous approach (11, 12). Specifically, the algebraic model results in far fewer dependent variables to be determined.

Model Development

The model presented here consists of a material balance for each component in every region and a charge balance for every region, as shown in Fig. 1. The major assumptions of this model are: (*i*) there is a diffusion region of known thickness in the electrolyte near each electrode, (*ii*) there is a perfectly mixed region a distance away from each electrode, and (*iii*) the electrolyte composition undergoes a step change from the inlet to the outlet composition within the reactor. This latter assumption is attributed to Mader and White (6) and is referred to by them as a "one-step" approximation. Other assumptions of this model are: (*i*) the system is isothermal, (*ii*) dilute solution theory applies, (*iii*) the flow is laminar in the reactor, and (*iv*) the Nernst-Einstein relationship (10) applies. The assumption of laminar flow within the reactor could be changed to turbulent flow, if desired. However, this would require that a turbulent velocity profile be used when determining the various average velocities throughout the reactor. It would also require that a turbulent velocity profile be used when determining the velocity-averaged concentrations.

In this model it is assumed that a parallel plate flow cell with a separator can be represented by the five regions shown in Fig. 1. These regions are: the region near the electrode on the anode side, the bulk region on the anode side, the separator region, the bulk region on the cathode side, and the region near the electrode on the cathode side. Additional regions could be added to the model. For example, diffusion regions near the separator/bulk region interfaces could be added. This was not done here because the gradients of the chemical species in these regions would be expected to be small (6). Each region can transfer material to the regions next to it through the processes of diffusion and migration, and each region except the separator has material carried into and out of it by the process of convection. For the purpose of simplicity, the velocity profile within each region is assumed to be uniform, and the average velocity for each region is determined by an integral-averaging method. Also for simplicity, the outlet concentration profiles for each region are assumed to be uniform, although these values are also determined by an integral-

* Electrochemical Society Student Member.
** Electrochemical Society Active Member.

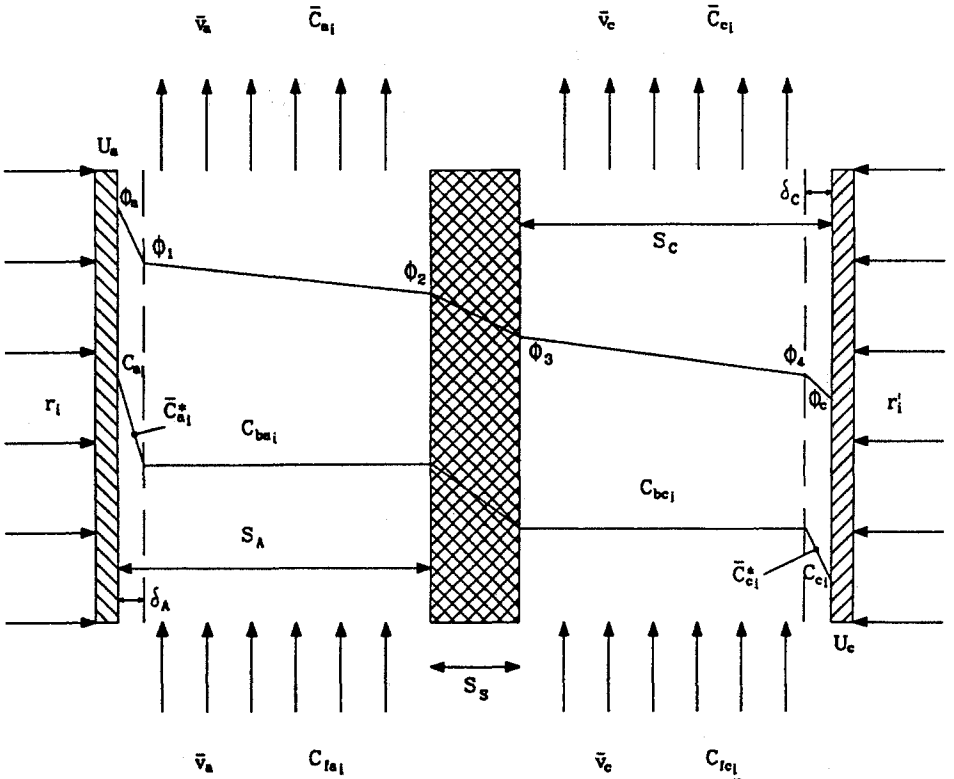

Fig. 1. Schematic of Zn/Br_2 flow cell under charge conditions.

averaging method. It is also assumed that the potential and concentration profiles within the regions near each electrode and within the separator are linear. Another assumption is that the bulk region of each flow channel is perfectly mixed, and as a result, the concentration profiles within each bulk region are flat. If the perfectly mixed assumption for the bulk region is correct, then it follows that the electrical resistivity in each bulk region is constant. Hence, it follows that the potential gradient within each bulk region must be constant.

Prior to developing the material balance equations for the reactor, it is necessary to determine the average fluid velocity in each of the regions of the reactor. This is done in a standard way in Appendix A (for each diffusion region) and in Appendix B (for each perfectly mixed region) of Ref. (14). The results are as follows

$$\bar{v}_{ea} = \frac{\bar{v}_a \delta_A}{S_A}\left(3 - 2\frac{\delta_A}{S_A}\right) \qquad [1]$$

$$\bar{v}_{ec} = \frac{\bar{v}_c \delta_C}{S_C}\left(3 - 2\frac{\delta_C}{S_C}\right) \qquad [2]$$

for each diffusion region (*i.e.*, within the δ_A and δ_C regions of Fig. 1) and

$$\bar{v}_{ba} = \frac{\bar{v}_a}{S_A - \delta_A}\left(S_A - 3\frac{\delta_A{}^2}{S_A} + 2\frac{\delta_A{}^3}{S_A{}^2}\right) \qquad [3]$$

$$\bar{v}_{bc} = \frac{\bar{v}_c}{S_C - \delta_C}\left(S_C - 3\frac{\delta_C{}^2}{S_C} + 2\frac{\delta_C{}^3}{S_C{}^2}\right) \qquad [4]$$

for each perfectly mixed region. It is also necessary to determine the average concentrations in each of the regions. These average concentrations are as follows

$$\bar{C}_{ea_i} = \frac{1}{2}(C_{a_i} + C_{ba_i}) \qquad [5]$$

for the volume-averaged concentrations near the anode

$$\bar{C}_{ec_i} = \frac{1}{2}(C_{c_i} + C_{bc_i}) \qquad [6]$$

for the volume-averaged concentrations near the cathode

$$\bar{C}_{s_i} = \frac{1}{2}(C_{ba_i} + C_{bc_i}) \qquad [7]$$

for the volume-averaged concentrations in the separator

$$\bar{C}^*_{a_i} = C_{a_i} + (C_{ba_i} - C_{a_i})\frac{(2 - 3\delta_A/2S_A)}{(3 - 2\delta_A/S_A)} \qquad [8]$$

for the velocity-averaged concentrations near the anode, and

$$\bar{C}^*_{c_i} = C_{c_i} + (C_{bc_i} - C_{c_i})\frac{(2 - 3\delta_C/2S_C)}{(3 - 2\delta_C/S_C)} \qquad [9]$$

for the velocity-averaged concentrations near the cathode. Equations [5-9] are derived in Ref. (14).

The material balance equations for the five regions between the electrodes are

$$\frac{d\bar{C}_{ea_i}}{dt} = \frac{r_i - N_{a_i}}{\delta_A} + \frac{\bar{v}_{ea}}{L}(C_{fa_i} - \bar{C}^*_{a_i}) + R_{ea_i}$$

(diffusion region near anode) [10]

$$\frac{dC_{ba_i}}{dt} = \frac{N_{a_i} - N_{sa_i}}{S_A - \delta_A} + \frac{\bar{v}_{ba}}{L}(C_{fa_i} - C_{ba_i}) + R_{ba_i}$$

(bulk region near anode) [11]

$$\frac{d\bar{C}_{s_i}}{dt} = \frac{N_{sa_i} - N_{sc_i}}{S_S} + R_{s_i} \quad \text{(separator)} \qquad [12]$$

$$\frac{dC_{bc_i}}{dt} = \frac{N_{sc_i} - N_{c_i}}{S_C - \delta_C} + \frac{\bar{v}_{bc}}{L}(C_{fc_i} - C_{bc_i}) + R_{bc_i}$$

(bulk region near cathode) [13]

$$\frac{d\bar{C}_{ec_i}}{dt} = \frac{N_{c_i} + r'_i}{\delta_C} + \frac{\bar{v}_{ec}}{L}(C_{fc_i} - \bar{C}^*_{c_i}) + R_{ec_i}$$

(diffusion region near cathode) [14]

Equations [10] and [11] are derived in the Appendixes A and B. Equations [12], [13], and [14] are derived in Appendixes G-I of Ref. [14].

Equations [10]-[14] contain one or more variables representing molar flux. These quantities are defined as follows

$$N_{a_i} = -D_i \frac{C_{ba_i} - C_{a_i}}{\delta_A} - z_i \mathbf{F} \frac{D_i}{RT} C_{ba_i} \frac{\phi_1 - \phi_a}{\delta_A} \quad [15]$$

$$N_{sa_i} = -\frac{D_i}{N_M} \frac{C_{bc_i} - C_{ba_i}}{S_S} - z_i \mathbf{F} \frac{D_i}{N_M RT} C_{ba_i} \frac{\phi_3 - \phi_2}{S_S} \quad [16]$$

$$N_{sc_i} = -\frac{D_i}{N_M} \frac{C_{bc_i} - C_{ba_i}}{S_S} - z_i \mathbf{F} \frac{D_i}{N_M RT} C_{bc_i} \frac{\phi_3 - \phi_2}{S_S} \quad [17]$$

$$N_{c_i} = -D_i \frac{C_{c_i} - C_{bc_i}}{\delta_C} - z_i \mathbf{F} \frac{D_i}{RT} C_{bc_i} \frac{\phi_c - \phi_4}{\delta_C} \quad [18]$$

Equations [10] and [14] contain one of two variables representing reaction rate. These reaction rates are Butler-Volmer kinetic expressions and are defined as follows

$$r_i = \beta \frac{s_{i,1} i_{o1,ref}}{n_1 \mathbf{F}} \left[\left(\frac{C_{a,Br^-}}{C_{ref,Br^-}} \right) \exp\left(\frac{\alpha_{a,1} \mathbf{F}}{RT} \eta_{a,1} \right) - \left(\frac{C_{a,Br_2}}{C_{ref,Br_2}} \right)^{0.5} \exp\left(\frac{-\alpha_{c,1} \mathbf{F}}{RT} \eta_{a,1} \right) \right] \quad [19]$$

$$\beta = \frac{A_{eff}}{A} \quad [20]$$

$$\eta_{a,1} = U_a - \phi_a - U_{ref,1} \quad [21]$$

$$r'_i = r'_{i,1} + r'_{i,2} \quad [22]$$

$$r'_{i,1} = \frac{s_{i,1} i_{o1,ref}}{n_1 \mathbf{F}} \left[\left(\frac{C_{c,Br^-}}{C_{ref,Br^-}} \right) \exp\left(\frac{\alpha_{a,1} \mathbf{F}}{RT} \eta_{c,1} \right) - \left(\frac{C_{c,Br_2}}{C_{ref,Br_2}} \right)^{0.5} \exp\left(\frac{-\alpha_{c,1} \mathbf{F}}{RT} \eta_{c,1} \right) \right] \quad [23]$$

$$r'_{i,2} = \frac{s_{i,2} i_{o2,ref}}{n_2 \mathbf{F}} \left[\exp\left(\frac{\alpha_{a,2} \mathbf{F}}{RT} \eta_{c,2} \right) - \left(\frac{C_{c,Zn^{+2}}}{C_{ref,Zn^{+2}}} \right)^{0.5} \exp\left(\frac{-\alpha_{c,2} \mathbf{F}}{RT} \eta_{c,2} \right) \right] \quad [24]$$

$$\eta_{c,j} = U_c - \phi_c - U_{ref,j} \quad [25]$$

$U_{ref,j}$ is the open-circuit potential for reaction j at reference conditions (6). The variable β is included in Eq. [19] to account for reaction in the porous electrode. It is defined as Eq. [20] because Evans and White (7) showed that the reaction at the bromine electrode is kinetically limited. Therefore, the concentration and potential profiles within the porous electrode are flat. As a result, the porous electrode simply increases the reaction rate at the bromine electrode, and a simple way to model this phenomena is to treat the electrode as though it had a larger surface area.

If Eq. [5] and [6] are substituted into Eq. [10] and [14], respectively, the following equations can be obtained after rearrangement

$$\frac{dC_{a_i}}{dt} = 2\left[\frac{r_i - N_{a_i}}{\delta_A} + \frac{\bar{v}_{ea}}{L} (C_{fa_i} - \bar{C}^*_{a_i}) + R_{ea_i} \right] - \frac{dC_{ba_i}}{dt} \quad [26]$$

$$\frac{dC_{c_i}}{dt} = 2\left[\frac{N_{c_i} + r'_i}{\delta_C} + \frac{\bar{v}_{ec}}{L} (C_{fc_i} - \bar{C}^*_{c_i}) + R_{ec_i} \right] - \frac{dC_{bc_i}}{dt} \quad [27]$$

If Eq. [11] and [13] are then substituted into Eq. [26] and [27], the following equations are obtained

$$\frac{dC_{a_i}}{dt} = 2\left[\frac{r_i - N_{a_i}}{\delta_A} + \frac{\bar{v}_{ea}}{L} (C_{fa_i} - \bar{C}^*_{a_i}) + R_{ea_i} \right] - \left[\frac{N_{a_i} - N_{sa_i}}{S_A - \delta_A} + \frac{\bar{v}_{ba}}{L} (C_{fa_i} - C_{ba_i}) + R_{ba_i} \right] \quad [28]$$

$$\frac{dC_{c_i}}{dt} = 2\left[\frac{N_{c_i} + r'_i}{\delta_C} + \frac{\bar{v}_{ec}}{L} (C_{fc_i} - \bar{C}^*_{c_i}) + R_{ec_i} \right] - \left[\frac{N_{sc_i} - N_{c_i}}{S_C - \delta_C} + \frac{\bar{v}_{bc}}{L} (C_{fc_i} - C_{bc_i}) + R_{bc_i} \right] \quad [29]$$

The charge balance equations for the reactor are

$$\Sigma z_i r_i + \frac{1}{\delta_A} \left[\Sigma z_i D_i (C_{ba_i} - C_{a_i}) + \frac{\mathbf{F}(\phi_1 - \phi_a)}{RT} \Sigma z_i^2 D_i C_{ba_i} \right] = 0 \quad [30]$$

for the diffusion region near the anode

$$\Sigma z_i r_i + \frac{\mathbf{F}(\phi_2 - \phi_1)}{RT(S_A - \delta_A)} \Sigma z_i^2 D_i C_{ba_i} = 0 \quad [31]$$

for the bulk region on the anode side

$$\Sigma z_i r_i + \frac{1}{N_M S_S} \left[\Sigma z_i D_i (C_{bc_i} - C_{ba_i}) + \frac{\mathbf{F}(\phi_3 - \phi_2)}{2RT} \Sigma z_i^2 D_i (C_{ba_i} + C_{bc_i}) \right] = 0 \quad [32]$$

for the separator

$$\Sigma z_i r_i + \frac{\mathbf{F}(\phi_4 - \phi_3)}{RT(S_C - \delta_C)} \Sigma z_i^2 D_i C_{bc_i} = 0 \quad [33]$$

for the bulk region on the cathode side

$$\Sigma z_i r_i + \frac{1}{\delta_C} \left[\Sigma z_i D_i (C_{c_i} - C_{bc_i}) + \frac{\mathbf{F}(\phi_c - \phi_4)}{RT} \Sigma z_i^2 D_i C_{bc_i} \right] = 0 \quad [34]$$

for the diffusion region near the cathode, and finally

$$\Sigma z_i (r_i + r'_i) = 0 \quad [35]$$

for the entire reactor. These charge balance relationships can be better understood by referring to Appendixes C and D. Equations [30]-[35] are derived in Appendixes J-O of Ref. (14).

The current density is defined as (10)

$$i = \mathbf{F} \Sigma z_i r_i = -\mathbf{F} \Sigma z_i r'_i \quad [36]$$

The voltage drop through the electrolyte during charge is defined as

$$\Delta\phi = \phi_a - \phi_c \quad [37]$$

Model Solution

Eq. [28], [11], [13], and [29] govern the time dependence of each of the n species concentrations in each of the four regions (δ_A, S_A, S_C, and δ_C) of the reactor. These $4n$ material balance equations plus the six current balance equations (*i.e.*, Eq. [30]-[35]) constitute a system of $4n + 6$ independent equations. These equations are in terms of $4n$ concentrations (C_{a_i}, C_{ba_i}, C_{bc_i}, and C_{c_i}) and six potentials (ϕ_a, ϕ_1, ϕ_2,

Table I. Butler-Volmer kinetic data (T = 298.15 K)

Reaction (j)	$i_{oj,ref}$ (A-cm^2)	α_{aj}	α_{cj}	n_j	U_j^θ (V)	$U_{ref,j}$ (V)
1	+0.31E − 02	0.5	0.5	1	+1.087	+1.783
2	+0.10E+ 01	0.5	0.5	1	−0.763	+0.000

Table II. Stoichiometry data

Species (i)	Reaction 1 $s_{i,j}$	Reaction 2 $s_{i,j}$
Na^+	+0.0	+0.0
Br^-	−1.0	+0.0
Br_2	+0.5	+0.0
Zn^{+2}	+0.0	+0.5
Br_3^-	+0.0	+0.0

Table III. Physical property data and feed composition

Species (i)	z_i	D_i (cm^2/s)	C_{f_i} (mol/cm^3)
Na^+	+1	+0.1334E − 04	+0.1000E − 02
Br^-	−1	+0.2084E − 04	+0.2949E − 02
Br_2	+0	+0.1310E − 04	+0.1015E − 05
Zn^{+2}	+2	+0.7540E − 05	+0.1000E − 02
Br_3^-	−1	+0.1310E − 04	+0.5100E − 04

Table IV. Comparison of predictions

	i (mA/cm^2)	$\Delta\phi$ (mV)	ϵ_T
Continuous model	20.02	15.35	0.586
"One-step" model	19.69	15.15	0.619
Algebraic model	20.12	15.45	0.491

ϕ_3, ϕ_4, and ϕ_c); therefore, there are a total of $4n + 6$ dependent variables. Hence, this system of equations completely describes any such reactor's performance for a constant set of feed compositions. For the steady-state case reported here, the $4n$ material balance equations (Eq. [28], [11], [13], and [29]) are set equal to zero, and the complete system of $4n + 6$ equations is solved using a Newton-Raphson procedure.

Prior to solving for the reactor's performance at steady state, all of the relevant operating conditions and reactor dimensions must be specified. These parameters include the following: C_{fa_i} and C_{fc_i} for each component, E_{cell} ($E_{cell} = U_a - U_c$), S_A and S_C ($S_A = S_C = S$ here), $N_M S_S$, δ_A and δ_C ($\delta_A = \delta_C = \delta$ here), $L/\bar{v}_a$ and $L/\bar{v}_c$ ($L/\bar{v}_a = L/\bar{v}_c$ here), and the physical properties for each of the components. Tables I-III list values for the input parameters used in this model. N_M represents the Macmullin number (6), which is defined as the resistivity of the separator soaked in electrolyte divided by the resistivity of that electrolyte.

The selection of values for the diffusion layer thicknesses is critical to this model. It may be possible to estimate values for these thicknesses by using boundary layer theory. It may also be possible to determine these values by experimental measurement. The authors estimated values for these thicknesses by comparing predictions from the model (using assumed values for the thicknesses) with predictions from previous models.

Once the steady-state conditions within the reactor have been predicted, the average outlet concentrations are readily determined by a material balance at the exit of the reactor. The resulting equations are

$$\bar{C}_{a_i} = \frac{\delta_A \bar{v}_{ea} \bar{C}^*_{a_i} + (S_A - \delta_A)\, \bar{v}_{ba} C_{ba_i}}{S_A \bar{v}_a} \quad [38]$$

$$\bar{C}_{c_i} = \frac{\delta_C \bar{v}_{ec} \bar{C}^*_{c_i} + (S_C - \delta_C)\, \bar{v}_{bc} C_{bc_i}}{S_C \bar{v}_c} \quad [39]$$

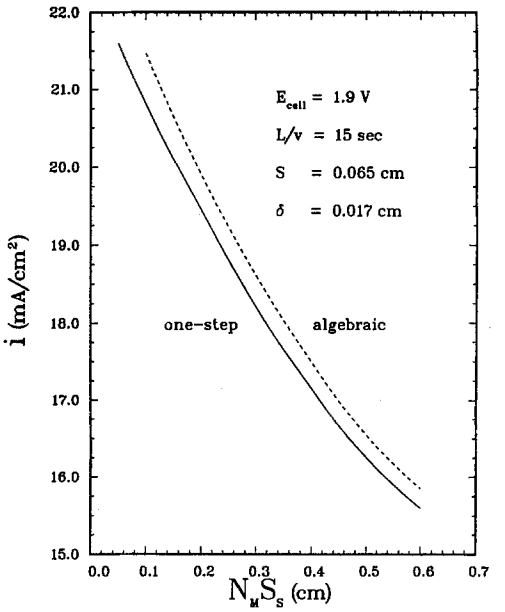

Fig. 2. Comparison of the current densities predicted by the one-step and algebraic models.

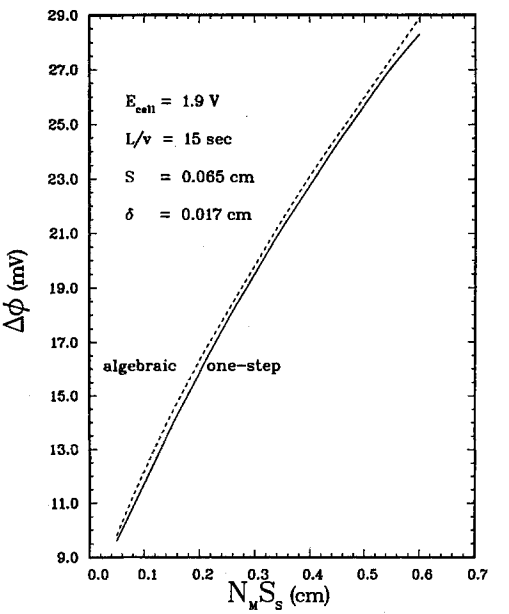

Fig. 3. Comparison of the voltage drops predicted by the one-step and algebraic models.

Once the outlet concentrations are determined, the conversions for each of the components can easily be determined from the following definitions

$$x_{a_i} = \frac{C_{fa_i} - \bar{C}_{a_i}}{C_{fa_i}} \quad [40]$$

$$x_{c_i} = \frac{C_{fc_i} - \bar{C}_{c_i}}{C_{fc_i}} \quad [41]$$

Discussion and Results

Figures 2 and 3 are comparisons of predictions obtained from Mader and White (6) and the model presented here. In both of these figures, the solid line represents the predictions obtained from Mader's "one-step" model, and the dashed line represent values obtained from the algebraic model. The comparison between the two models is good (within about 2%) throughout the entire range of effective separator thicknesses investigated. Table IV presents a direct comparison of predictions made using the algebraic model, Mader's "one-step" model, and Mader's continuous

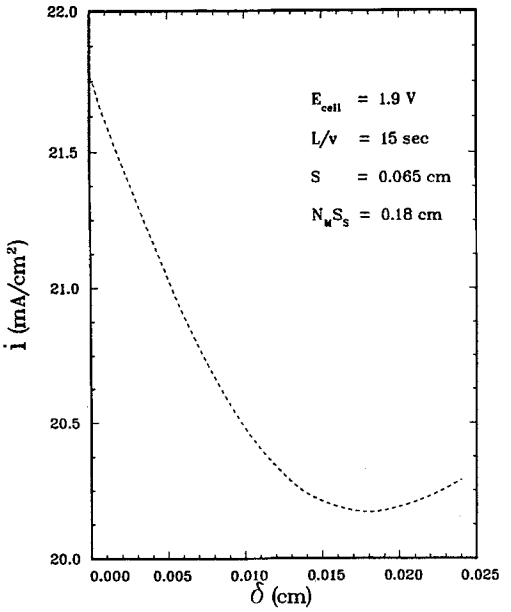

Fig. 4. Predicted current density vs. diffusion layer thickness for the algebraic model.

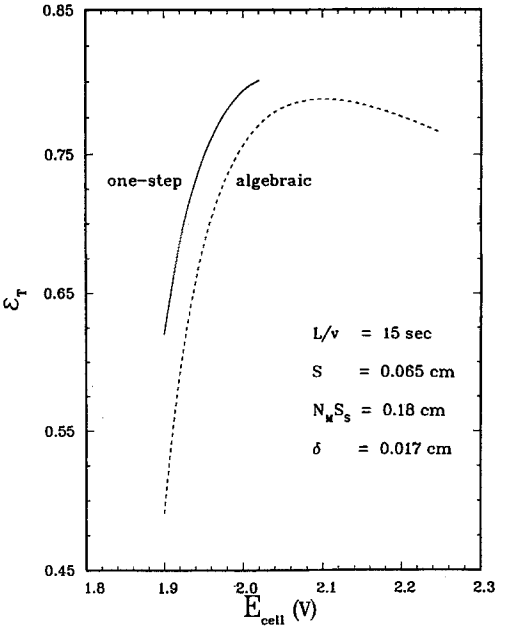

Fig. 6. Comparison of the total efficiencies predicted by the one-step and algebraic models.

model. Surprisingly, the algebraic model predicts values for i and $\Delta\phi$ that are closer to those predicted by the continuous model than does the "one-step" model. However, the value for the total efficiency (see Eq. [41] of Ref. (6)) predicted by the algebraic model differs significantly from the values predicted by both of Mader's models. This discrepancy is most likely due to the tremendous difference in the values of the exchange current densities for the zinc and bromine reactions at the zinc electrode (see Table I).

Figure 4 shows how the predicted current density for the cell depends on various assumed values of the diffusion layer thickness. It is apparent from Fig. 4 that the calculated value of the current density depends on the assumed value of the diffusion layer thickness; however, this dependence is weak (about 8% maximum change). This dependence could be used to the experimental data to fit model predictions by adjusting the value of δ.

Figure 5 shows the effect of E_{cell} upon the current efficiency at the cathode. The current efficiency at the cathode is strongly influenced by the operating potential, and it should approach unity for very high values of E_{cell}. These two findings are attributed to the tremendous difference between the values of the exchange current densities for the two reactions at the cathode. Figure 6 shows the effect of E_{cell} upon the total energy efficiency of the cell. It is apparent from Fig. 6 that there is an optimum value for the cell potential at which the battery should be operated so that the maximum amount of energy can be stored. This maximum occurs because the total efficiency is the product of the current efficiency and the voltaic efficiency. Although the current efficiency increases monotonically with respect to E_{cell}, the voltaic efficiency decreases monotonically with respect to E_{cell}. For this system there is a point beyond which any increase in the current efficiency is more than offset by the associated decrease in the voltaic efficiency. For the feed composition studied, the maximum energy efficiency occurs at about 2.10V. Mader (13) presents figures similar to Fig. 5 and 6. Unfortunately, he does not present data beyond 2.03V. As a result, he did not report that the total efficiency has a maximum value.

Figures 7 and 8 show the effect of varying β (*i.e.*, the area ratio) for the porous bromine electrode. It seems reasona-

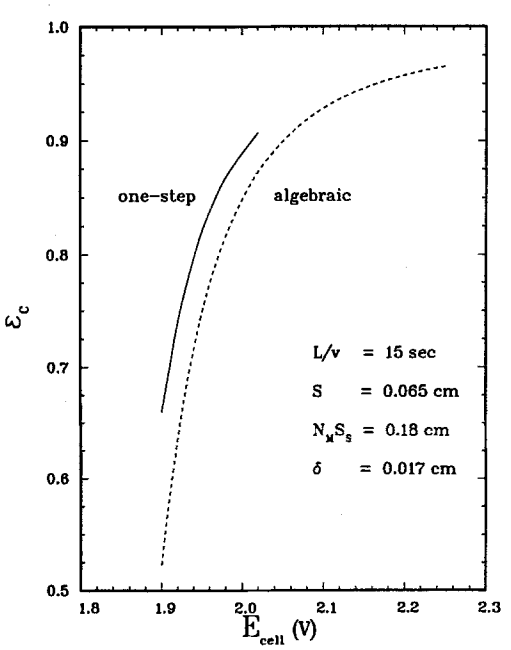

Fig. 5. Comparison of the current efficiencies predicted by the one-step and algebraic models.

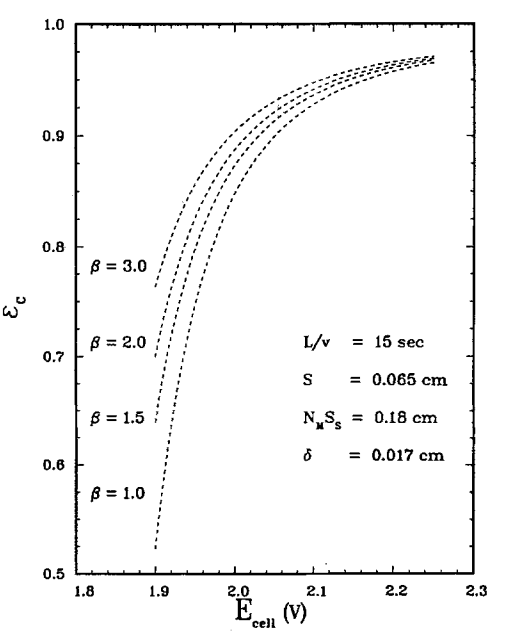

Fig. 7. Predicted current efficiency vs. cell potential for several values of β.

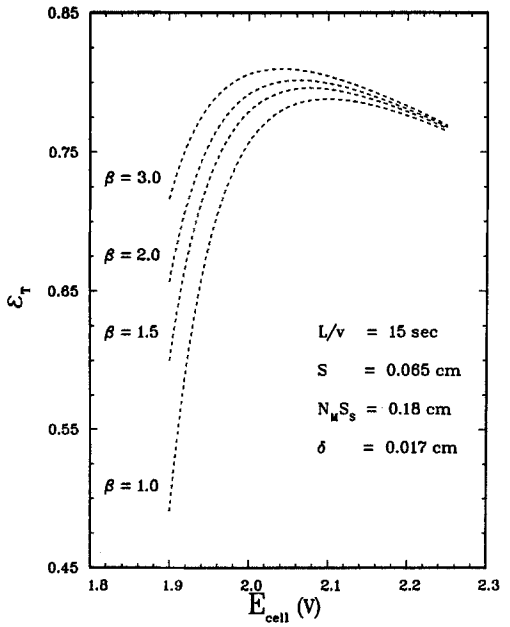

Fig. 8. Predicted total efficiency vs. cell potential for several values of β.

ble that higher efficiencies would be obtained by reactors with porous electrodes, because the increased surface area results in a higher production rate of Br_2 during charge, and this higher production rate results in a higher current density at the anode. Since the current density at the anode is higher, it follows that the current density at the cathode must also be higher, and the only way for that to occur is for the overpotential at the cathode to increase. Such an increase of overpotential greatly favors the zinc reaction (because of the values of the exchange current densities); therefore, the current efficiency increases.

It is likely that the optimum value of E_{cell} at which the maximum total efficiency occurs is influenced by the feed composition. If this is true, then it follows that for a system where the feed composition changes with time (such as the zinc/bromine battery), the optimum value of E_{cell} would also change with time. The occurrence of an optimum E_{cell} is a very practical result that may be applicable to all parallel plate cells with multiple reactions at one or more of the electrodes.

Conclusions

This paper demonstrates that a parallel plate flow cell can be approximated by a combination of perfectly mixed regions and diffusion regions. For a reactor that incorporates a porous separator and has a low conversion (such as the zinc/bromine battery), the reactor can be approximated at steady state by $4n + 6$ variables. If the porous separator were not present in the system, the reactor could be approximated at steady state by $3n + 4$ variables. Also, this paper presents a set of ordinary differential equations that describe the performance of a parallel flow cell at unsteady state. These equations should be solvable by a Runge-Kutta technique, and such a solution may be the subject of a future paper.

This paper also shows that an optimum value of E_{cell} may exist for a zinc/bromine battery. For the feed composition studied, the optimum cell potential is about 2.10V. Such an optimum may also exist for other systems with multiple electrode reactions. For the zinc/bromine system, the optimum cell potential may be influenced by the feed composition. If this is true, then the value of E_{cell} would have to be constantly varied for the battery to be operated in the most efficient manner.

Acknowledgment

The authors wish to acknowledge the support of this work by the National Science Foundation through Grant No. CBT-8620142.

Manuscript submitted June 6, 1988; revised manuscript received Dec. 12, 1988.

Texas A&M University assisted in meeting the publication costs of this article.

LIST OF SYMBOLS

A	(cm^2) projected area of porous electrode
A_{eff}	(cm^2) effective area of porous electrode
C_{ba_i}	(mol/cm^3) bulk region concentration on anode side
C_{bc_i}	(mol/cm^3) bulk region concentration on cathode side
C_{fa_i}	(mol/cm^3) feed concentration on anode side
C_{fc_i}	(mol/cm^3) feed concentration on cathode side
$\bar{C}_{a_i}$	(mol/cm^3) average outlet concentration on anode side
$\bar{C}_{c_i}$	(mol/cm^3) average outlet concentration on cathode side
$\bar{C}_{s_i}$	(mol/cm^3) average concentration is separator
$\bar{C}_{ea_i}$	(mol/cm^3) average concentration near electrode on anode side
$\bar{C}_{ec_i}$	(mol/cm^3) average concentration near electrode on cathode side
$\bar{C}^*_{a_i}$	(mol/cm^3) velocity-averaged concentration near the anode
$\bar{C}^*_{c_i}$	(mol/cm^3) velocity-averaged concentration near the cathode
$C_{ref,i}$	(mol/cm^3) reference concentration
D_i	(cm^2/s) diffusion coefficient
E_{cell}	(V) operating potential of reactor
F	**(C/mol) Faraday's constant (96,487 C/*M*)**
i	(mA/cm^2) total current density
$i_{oj,ref}$	(mA/cm^2) exchange current density for j'th reaction at referenced concentration
L	(cm) reactor length
n	number of components
n_j	number of electrons in the j'th electrochemical reaction
N_M	Macmullin number
N_{a_i}	(mol/cm^2 s) mole flux from anode region into anode bulk region
N_{c_i}	(mol/cm^2) mole flux from cathode bulk region into cathode region
N_{sa_i}	(mol/cm^2) mole flux from anode bulk region into separator
N_{sc_i}	(mol/cm^2 s) mole flux from separator into cathode bulk region
q_A	(cm^3/s) volumetric flow rate through anode side
q_C	(cm^3/s) volumetric flow rate through cathode side
R	(J/mol K) gas constant (*i.e.*, 8.314 J/mol K)
r_i	(mol/cm^2 s) reaction rate at anode surface (from Butler-Volmer equation)
r'_i	(mol/cm^2 s) reaction rate at cathode surface (from Butler-Volmer equation)
R_{ea_i}	(mol/cm^3 s) homogeneous reaction rate in diffusion region near anode
R_{ec_i}	(mol/cm^3 s) homogeneous reaction rate in diffusion region near anode
R_{ba_i}	(mol/cm^3 s) homogeneous reaction rate in bulk near anode
R_{bc_i}	(mol/cm_3 s) homogeneous reaction rate in bulk near cathode
R_{s_i}	(mol/cm^3 s) homogeneous reaction rate in separator
$s_{i,j}$	stoichiometric coefficient
S_A	(cm) distance from anode surface to separator
S_C	(cm) distance from cathode surface to separator
S_S	(cm) distance across separator
T	(K) reactor temperature
$U_{ref,j}$	(V) reference potential for reaction j
U_j^θ	(V) half-cell potential for reaction j
U_a	(V) potential at anode
U_c	(V) potential at cathode
V_{TA}	(cm^3) volume of storage bulk tank on anode side
V_{TC}	(cm^3) volume of storage tank on cathode side
$\bar{v}_a$	(cm/s) average velocity through anode side
$\bar{v}_c$	(cm/s) average velocity through cathode side
$\bar{v}_{ba}$	(cm/s) average velocity in bulk region on anode side
$\bar{v}_{bc}$	(cm/s) average velocity in bulk region on cathode side
$\bar{v}_{ea}$	(cm/s) average velocity near electrode on anode side
$\bar{v}_{ec}$	(cm/s) average velocity near electrode on cathode side
W	(cm) reactor width

α_{aj} apparent anodic transfer coefficient for reaction j
α_{cj} apparent cathodic transfer coefficient for reaction j
z_i ionic charge
β area ratio for porous electrode (A_{eff}/A)
δ_A (cm) diffusion layer thickness near anode
δ_C (cm) diffusion layer thickness near cathode
η_a (V) overpotential at the anode
η_c (V) overpotential at the cathode
ϕ_a (V) electrolyte potential at anode surface
ϕ_c (V) electrolyte potential at cathode surface
ϕ_1 (V) electrolyte potential at interface between diffusion region and perfectly mixed region on anode side
ϕ_2 (V) electrolyte potential at separator on anode side
ϕ_3 (V) electrolyte potential at separator on cathode side
ϕ_4 (V) electrolyte potential at interface between diffusion region and perfectly mixed region on cathode side
$\Delta\phi$ (V) voltage drop through electrolyte and separator
ϵ_C current efficiency (6)
ϵ_T total efficiency (6)

APPENDIX A

Figure A-1 is a schematic of the mole fluxes that enter and leave the diffusion region near the anode

$$N_{a_i} = -D_i \frac{C_{ba_i} - C_{a_i}}{\delta_A} - z_i \mathbf{F} \frac{D_i}{RT} C_{ba_i} \frac{\phi_1 - \phi_a}{\delta_A}$$

A verbal statement of the material balance is

(moles in) − (moles out)

+ (moles generated) = (moles accumulated)

where

(moles in) = $[r_i LW + C_{fa_i} \bar{v}_{ea} \delta_A W]\, \Delta t$

(moles out) = $[N_{a_i} LW + \bar{C}^*_{a_i} \bar{v}_{ea} \delta_A W)\, \Delta t$

(moles generated) = $R_{ea_i} L \delta_A W \Delta t$

(moles accumulated) = $[\bar{C}_{ea_i}(t + \Delta t) - \bar{C}_{ea_i}(t)]\, L \delta_A W$

Substitution of these definitions into the verbal material balance yields

$$[r_i LW + C_{fa_i} \bar{v}_{ea} \delta_A W - (N_{a_i} LW + \bar{C}^*_{a_i} \bar{v}_{ea} \delta_A W) + R_{ea_i} L \delta_A W]\, \Delta t = [\bar{C}_{ea_i}(t + \Delta t) - \bar{C}_{ea_i}(t)]\, L \delta_A W \quad \text{[A-1.1]}$$

Rearangement of Eq. [A-1.1] yields the following

$$\frac{r_i - N_{a_i}}{\delta_A} + \frac{\bar{v}_{ea}}{L}(C_{fa_i} - \bar{C}^*_{a_i}) + R_{ea_i} = \frac{\bar{C}_{ea_i}(t + \Delta t) - \bar{C}_{ea_i}(t)}{\Delta t} \quad \text{[A-1.2]}$$

Taking the limit of Eq. [A-1.2] as Δt approaches zero yields

$$\frac{r_i - N_{a_i}}{\delta_A} + \frac{\bar{v}_{ea}}{L}(C_{fa_i} - \bar{C}^*_{a_i}) + R_{ea_i} = \frac{d\bar{C}_{ea_i}}{dt}$$

APPENDIX B

Figure A-2 is a schematic of the mole fluxes that enter and leave the bulk region on the anode side

$$N_{a_i} = -D_i \frac{C_{ba_i} - C_{a_i}}{\delta_A} - z_i \mathbf{F} \frac{D_i}{RT} C_{ba_i} \frac{\phi_1 - \phi_a}{\delta_A}$$

$$N_{sa_i} = -\frac{D_i}{N_M} \frac{C_{bc_i} - C_{ba_i}}{S_S} - z_i \mathbf{F} \frac{D_i}{N_M RT} C_{ba_i} \frac{\phi_3 - \phi_2}{S_S}$$

A verbal statement of the material balance is

(moles in) − (moles out)

+ (moles generated) = (moles accumulated)

where

(moles in) = $[N_{a_i} LW + C_{fa_i} \bar{v}_{ba}(S_A - \delta_A)\, W]\, \Delta t$

(moles out) = $[N_{sa_i} LW + C_{ba_i} \bar{v}_{ba}(S_A - \delta_A)\, W\, \Delta t$

(moles generated) = $R_{ba_i} L(S_A - \delta_A)\, W \Delta t$

(moles accumulated) = $[C_{ba_i}(t + \Delta t) - C_{ba_i}(t)]\, L(S_A - \delta_A)\, W$

Let $S = S_A - \delta_A$. Substitution of these definitions into the verbal material balance yields

$$[N_{a_i} LW + C_{fa_i} \bar{v}_{ba} SW - (N_{sa_i} LW + C_{ba_i} \bar{v}_{ba} SW) + R_{ba_i} LSW]\, \Delta t = [C_{ba_i}(t + \Delta t) - C_{ba_i}(t)]\, LSW \quad \text{[A-2.1]}$$

Rearrangement of Eq. [A-2.1] yields the following

$$\frac{N_{a_i} - N_{sa_i}}{S_A - \delta_A} + \frac{\bar{v}_{ba}}{L}(C_{fa_i} - C_{ba_i}) + R_{ba_i} = \frac{C_{ba_i}(t + \Delta t) - C_{ba_i}(t)}{\Delta t} \quad \text{[A-2.2]}$$

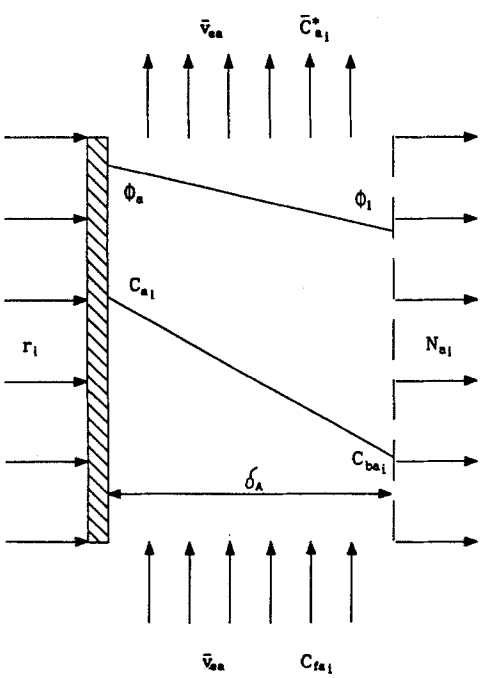

Fig. A-1. Material balance schematic of the diffusion region near the anode.

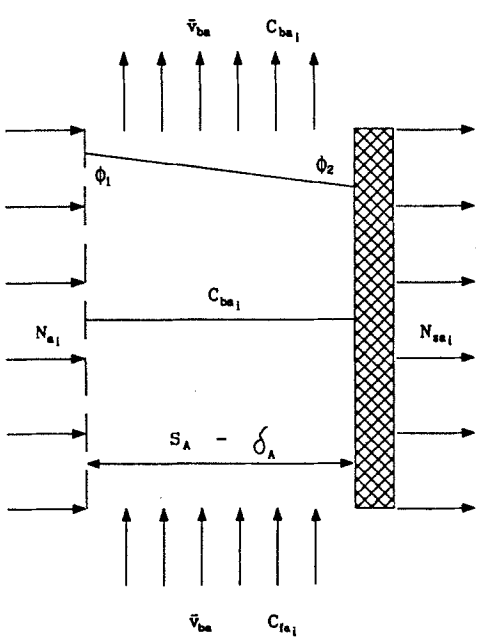

Fig. A-2. Material balance schematic of the bulk region on the anode side.

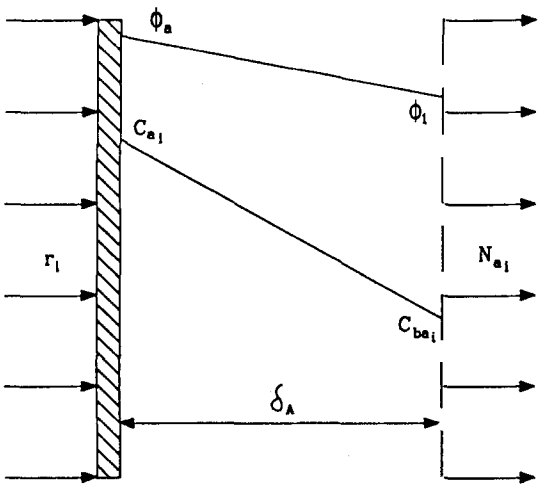

Fig. A-3. Charge balance schematic of the diffusion region near the anode.

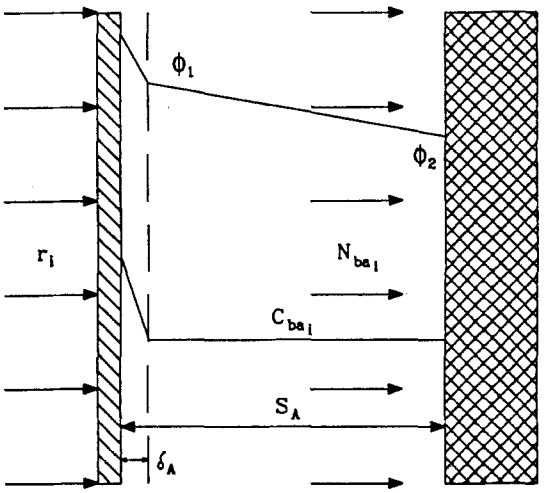

Fig. A-4. Charge balance schematic of the bulk region on the anode side.

Taking the limit of Eq. [A-2.2] as Δt approaches zero yields the following

$$\frac{N_{a_i} - N_{sa_i}}{S_A - \delta_A} + \frac{\bar{v}_{ba}}{L}(C_{a_i} - \bar{C}^*_{ba_i}) + R_{ba_i} = \frac{dC_{ba_i}}{dt}$$

APPENDIX C

Figure A-3 is a schematic of the charge fluxes that enter and leave the diffusion region near the anode

$$N_{a_i} = -D_i\frac{C_{ba_i} - C_{a_i}}{\delta_A} - z_i\mathbf{F}\frac{D_i}{RT}C_{ba_i}\frac{\phi_1 - \phi_a}{\delta_A}$$

A verbal statement of the charge balance is

(charge in) − (charge out) = 0

where

(charge in) = $\mathbf{F}LW\Sigma z_i r_i$

(charge out) = $\mathbf{F}LW\Sigma z_i N_{a_i}$

Substitution of these definitions into the verbal charge balance yields

$$\mathbf{F}LW\Sigma z_i r_i - \mathbf{F}LW\Sigma z_i N_{a_i} = 0 \qquad [A\text{-}3.1]$$

Simplification and substitution of the flux expression into Eq. [A-3.1] yield

$$\Sigma z_i r_i - \Sigma z_i\left(-D_i\frac{C_{ba_i} - C_{a_i}}{\delta_A} - z_i\mathbf{F}\frac{D_i}{RT}C_{ba_i}\frac{\phi_1 - \phi_a}{\delta_A}\right) = 0 \qquad [A\text{-}3.2]$$

Rearrangement of Eq. [A-3.2] yields the following

$$\Sigma z_i r_i + \frac{1}{\delta_A}\left[\Sigma z_i D_i(C_{ba_i} - C_{a_i}) + \frac{\mathbf{F}(\phi_1 - \phi_a)}{RT}\Sigma z_i^2 D_i C_{ba_i}\right] = 0$$

APPENDIX D

Figure A-4 is a schematic of the charge fluxes that enter and leave the bulk region on the anode side

$$N_{ba_i} = -z_i\mathbf{F}\frac{D_i}{RT}C_{ba_i}\frac{\phi_2 - \phi_1}{S_A - \delta_A}$$

A verbal statement of the charge balance is

(charge in) − (charge out) = 0

where

(charge in) = $\mathbf{F}LW\Sigma z_i r_i$

(charge out) = $\mathbf{F}LW\Sigma z_i N_{ba_i}$

Substitution of these definitions into the verbal charge balance yields

$$\mathbf{F}LW\Sigma z_i r_i - \mathbf{F}LW\Sigma z_i N_{ba_i} = 0 \qquad [A\text{-}4.1]$$

Substituting the flux expression into Eq. [A-4.1] yields

$$\Sigma z_i r_i - \Sigma z_i\left(-z_i\mathbf{F}\frac{D_i}{RT}C_{ba_i}\frac{\phi_2 - \phi_1}{S_A - \delta_A}\right) = 0 \qquad [A\text{-}4.2]$$

Rearrangement of Eq [A-4.2] yields the following

$$\Sigma z_i r_i + \frac{\mathbf{F}(\phi_2 - \phi_1)}{RT(S_A - \delta_A)}\Sigma z_i^2 D_i C_{ba_i} = 0$$

REFERENCES

1. M. Eigen and K. Kustin, *J. Am. Chem. Soc.*, **84,** 1355 (1962).
2. J. Lee and J. R. Selman, *This Journal*, **129,** 1670 (1982).
3. J. Lee and J. R. Selman, *ibid.*, **130,** 1237 (1983).
4. J. Lee, Ph.D. Dissertation, Illinois Institute of Technology, Chicago, IL (1981).
5. J. W. Van Zee, R. E. White, P. Grimes, and R. Bellows, in "Electrochemical Cell Design," R. E. White, Editor, p. 293, Plenum Publishing Co., New York (1984).
6. M. J. Mader and R. E. White, *This Journal*, **133,** 1297 (1986).
7. T. I. Evans and R. E. White, *ibid.*, **134,** 866 (1987).
8. T. I. Evans and R. E. White, *ibid.*, **134,** 2725 (1987).
9. D. J. Pickett, "Electrochemical Reactor Design," Chap. 4-6, Elsevier Scientific Publishing Co., New York (1979).
10. J. S. Newman, "Electrochemical Systems," Chap. 11, Prentice-Hall, Inc., Englewood Cliffs, NJ (1973).
11. V. Edwards and J. S. Newman, *This Journal*, **134,** 1181 (1987).
12. T. V. Nguyen, C. W. Walton, and R. E. White, *ibid.*, **133,** 1130 (1986).
13. M. J. Mader, M. S. Thesis, Texas A&M University, College Station, TX (1986).
14. G. D. Simpson, M. S. Thesis, Texas A&M University, College Station, TX (1988).